PCB-Integrated Embedded Planar Magnetorquers for Small Satellites Intelligent Detumbling

Shoaib Ahmed Khan[1], Yang Shiyou[1*], Anwar Ali[2], Mustafa Tahir[1], Shah Fahad[1], Shaowei Rao[1], Muhammad Waseem[1]
[1] College of Electrical Engineering, Zhejiang University, Hangzhou, 310027, China
[2] Department of electronics and electrical engineering, Faculty of Science and Engineering, Swansea University Bay Campus Swansea, UK
[1*]Corresponding Author Email: eesyyang@zju.edu.cn

Abstract- The challenge of damping high tumbling rates after deployment of spacecraft from a rocket using PCB-integrated (printed circuit board) embedded planar coils that acts as pseudo- 2D magnetorquers is explored for higher form factor small satellites (2U and 4U). The magnetorquers cannot generate the torque if their axes are lined up with the local geomagnetic field and generally the reaction wheels are actuated to generate this torque component. CubeSats are small satellites that have cube units of 10cm along each axis and they are usually detumbled using magnetorquer rods bringing norm to the point where reaction wheels take over to reduce the body rates to zero. In this paper, the task of removing the initial angular velocities is undertaken by using the embedded planar coils without relying on the secondary actuators using an intelligent projection based form of the B-Dot control. The proposed reconfigurable planar coils can effectively detumble the higher form factor small satellites using application-specific optimal coil configuration. The performance parameters for various possible combinations of the coils are thermally evaluated to sustain a stable thermal profile as the planar coils are embedded inside the multilayered PCB in the form of copper traces. Lastly, the proposed coils are compared with the performance parameters of the commercial actuators in the formal studies. It is found that the suggested embedded planar magnetorquers outperforms the competition.

***Index Terms*—Nanosatellites, embedded magnetorquer, attitude control, thermal analysis, detumbling.**

1. Introduction

At the dawn of the space age, the spacecraft were small because of the limited thrust capacities of early launch vehicles. The mass of the early spacecrafts such as Intelsat-1 or Explorer-1 ranged less than 15 and 39 kilograms respectively. Due to the demanding economies and rising global demand, spacecraft became more and more massive as rocket systems and launchers could support larger experimental payloads for carrying out more complex missions [1]. However, this makes the spacecraft very time-consuming and expensive to build. The tasks that were undertaken by the conventional larger spacecraft are now being performed by the small satellites because of the ongoing trend in the advancement and deployment of miniaturized spacecraft, such as remote sensing, communications, meteorology, Earth observation, defense applications and navigations [2]. The miniaturized spacecraft industry has seen tremendous rise over the last decade . The industry is now primed for growth achieving extraordinary recognition because of the spacecraft's miniaturization of dimensions and with the proposal of new constellations of more than thousand spacecraft [3]. Governments are reevaluating the small spacecraft market as commercial users rely on them for their cutting-edge technology's rapid development, flexibility, resilience, modularity, and risk-tolerance. Modern small satellites are usually one-hundredth of the cost and mass of the conventional satellites [4]. The development of modern miniaturized spacecraft stems from the motivation of two reasons; the first being the political and financial requirements for reducing the expenses and the second one involves the technological advancement in low-power microelectromechanical systems (MEMS) and digital signal processing (DSP) [5]. Very-large-scale integration (VLSI) revolutionized the realization of building advanced circuits into smaller volumes, with lesser power consumption and masss. Universities and research institutions jumped on the bandwagon realizing the need of fulfilling the societal functions in providing the engineering, testing and design verification to systems that could provide more than educational experience and ultimately be brought to fruition for higher form factor satellites [6,7]. Private industrial organizations like, Blue origin, Rocketplane Kistler, SpaceX are keenly providing services in the commercial orbital transportation service programs. While the United States has dominated 40% market, the rest of the world is also strengthening its space programs at enormous rates. The number of small spacecraft launched from 1974 to 2016 is 849 in which United States alone is responsible for launching over 201 small spacecraft. The launches included defense, commercial, scientific and university programs. The number of small spacecraft launched from 2000 to 2016 has seen an increase of almost 100% and in 2016 alone 92 small satellites were launched [3].

Small satellites can be further categorized in the classification of nano-and microsatellites by volume. 1U is a 1-unit CubeSat with a $10cm^3$ volume and they are further found in the range of units such as 1U, 3U or even 12U [8]. CubeSats weighing 1-20kg are being frequently built because of having lesser development times and cost effective modular architecture but although advances have certainly been made in microelectronics, many risks are also associated with these miniaturized systems such as, high probability of failure (40%), accommodating large number of subsystems in highly miniaturized dimensions and poor life expectancy. Similarly, the failure challenges faced by the attitude control systems (ACS) are also in dire need of robust architectures [9] capable of overcoming the harsh environmental disturbances such as gravity gradient and aerodynamic drags & torques and single even latch-up failures. With the advent of space exploration, magnetic actuators have been extensively used in the satellites that is simply based on the interaction of spacecraft's actuator magnetic field and the Earth's magnetic field [10]. The spacecraft is actuated using passive (hysteresis rods, permanent magnets) and active (magnetorquers, thrusters, reaction wheels) actuators [11]. Passive actuators rely on the gravity gradients, forces of external torques, solar radiation pressure and permanent magnets. Because of the lack of moving parts, passive systems consume no power consumption owing to its simple design but their pointing accuracy is subpar limiting their use in missions that require precise attitude maneuvers. Magnetic actuators are reliable,

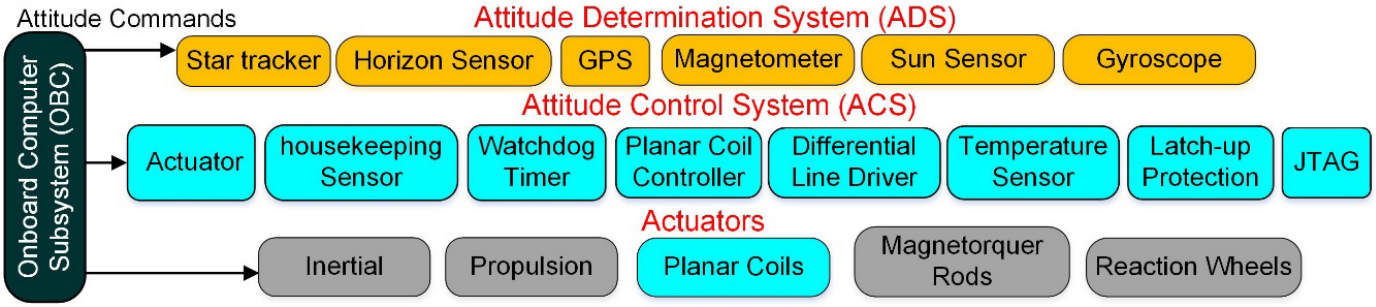

Fig. 1 The intercommunication of ACS and ADS with onboard computer system (OBC)

cheap, have low-mass and dissipate less power but the attitude stabilization based on these systems pose many issues as the generated torque by the magnetorquers is restricted on the axis perpendicular to the geomagnetic field's local direction whereas the reaction wheel/momentum wheels generates three dimensional torque but they are heavy and expensive [12]. The inherent under-actuation issue faced by the magnetic control is another major complication, providing limited available processing power as a result of restricted torques [13]. The issue is investigated by the combined use of gravity gradient and magnetic ACS for microspacraft [14]. The authors further investigate the issue for the problem of magnetic attitude tracking control and the method of predicted attitude trajectory in [15]. In orbital transfer, complicated dynamic behavior is shown for the gravity gradient based microsatellite under a constant thrust. A predicted attitude trajectory is devised based on dynamic characteristics in their results for damping out the vehicles' pendular motion to ensure reduced consumption of power and flight safety of the system. Figure 1 shows the block level intercommunication between the ACS and attitude determination system (ADS).

In the last decade, a major research and technology focus has been on the flight demonstration components to build robust and reliable satellite propulsion systems or thrusters. LituanicaSAT-2 was successfully launched recently which is built by joint effort between the Vilnius University & NanoAvionics and showed the propulsion systems' efficacy for the miniaturized spacecraft as a suitable choice. LithuanicaSAT-2- a 3U Lithuanian CubeSat was tested in orbit in 2017 and is a part of network of 50 CubeSat constellation for a mission of "QB50" led by Von Karman Institute, Belgium, deployed in sun- synchronous orbit at an altitude of 475 km [16]. Numerous companies are working to accelerate the electric propulsion (EP) infrastructure expansion in space through the development of high performance low-cost EP systems for small satellites [17]. However, because of their high pointing accuracies, there are constraints that limit the potential of the EP systems. For instance, unless a sophisticated magnetic confinement system is used, the ion thrusters' mechanism has a size limit beyond which the generated thrust can no longer be improved [18]. Some propulsion systems involve high complexity [19], necessitate miniaturized power processing units and still do not provide sufficient thrusts [20]; each system has its own challenges, which are being addressed by the ongoing research trend.

The moving parts in the reaction/momentum wheels, thrusters and gyroscopes cause majority (approximately 50%) of the faults in the attitude and orbital control systems (AOCS) [21]. These commercial off the shelf (COTS) based systems produce decent magnetic dipole moments but they occupy a larger space on the vehicle that is already aimed to be highly miniaturized. Magnetorquers are generally used for the detumbling of the spacecraft at sufficient levels to the instance when the momentum/reaction wheels are actuated bringing the norm to the point where the magnetorquers are again actuated to desaturate the momentum/reaction wheels. Mughal et al and Anwar et al in [22,23] used an interesting approach in the form of pseudo-2D-PCB integrated planar coils embedded inside the inner PCB layers to replace the bulky 3D magnetorquer rods, providing reasonable magnetic moments for the attitude maneuverability and stabilization in low Earth orbit (LEO). However, these embedded designs have not yet been investigated for removing the body rates of the satellites's initial angular velocities after deployment from the launcher, the contribution which will be undertaken in this paper.

This work proposes PCB integrated reconfigurable planar coils for the detumbling of higher form factor small satellites. The actuation capabilities for single axis attitude maneuvers were investigated in [22,23]. However, the basic idea of using these embedded designs is the occupation of almost no additional space in the spacecraft and the inability of detumbling the vehicle will require supplementary actuators for performing that operation. So, the problem of tumbling angular velocities with high inertias for CubeSats is analyzed in detail for the proposed planar coils. In this paper, the widely used projection based form of the standard B-dot control, reported in many sources, is selected for the spacecraft's detumbling which has the advantage of requiring less computational capacity of the onboard computer subsystem (OBC) [24,25]. The paper is structured as follows: Section 2 provides the module description of planar magnetorquer and its reconfigurability. Section 3 presents the analytical model of magnetorquer's attitude equations of motion along with the mathematical model for single axis maneuvering rotation times of various possible planar coil combinations. Section 4 describes the detumbling of small satellites actuated with various planar magnetorquers. Section 5 explains thermal gradients of magnetorquers in detail to validate the heat transfer's safety and a comparison is done with the best-case designs.

2. PCB integrated planar magnetorquer driver

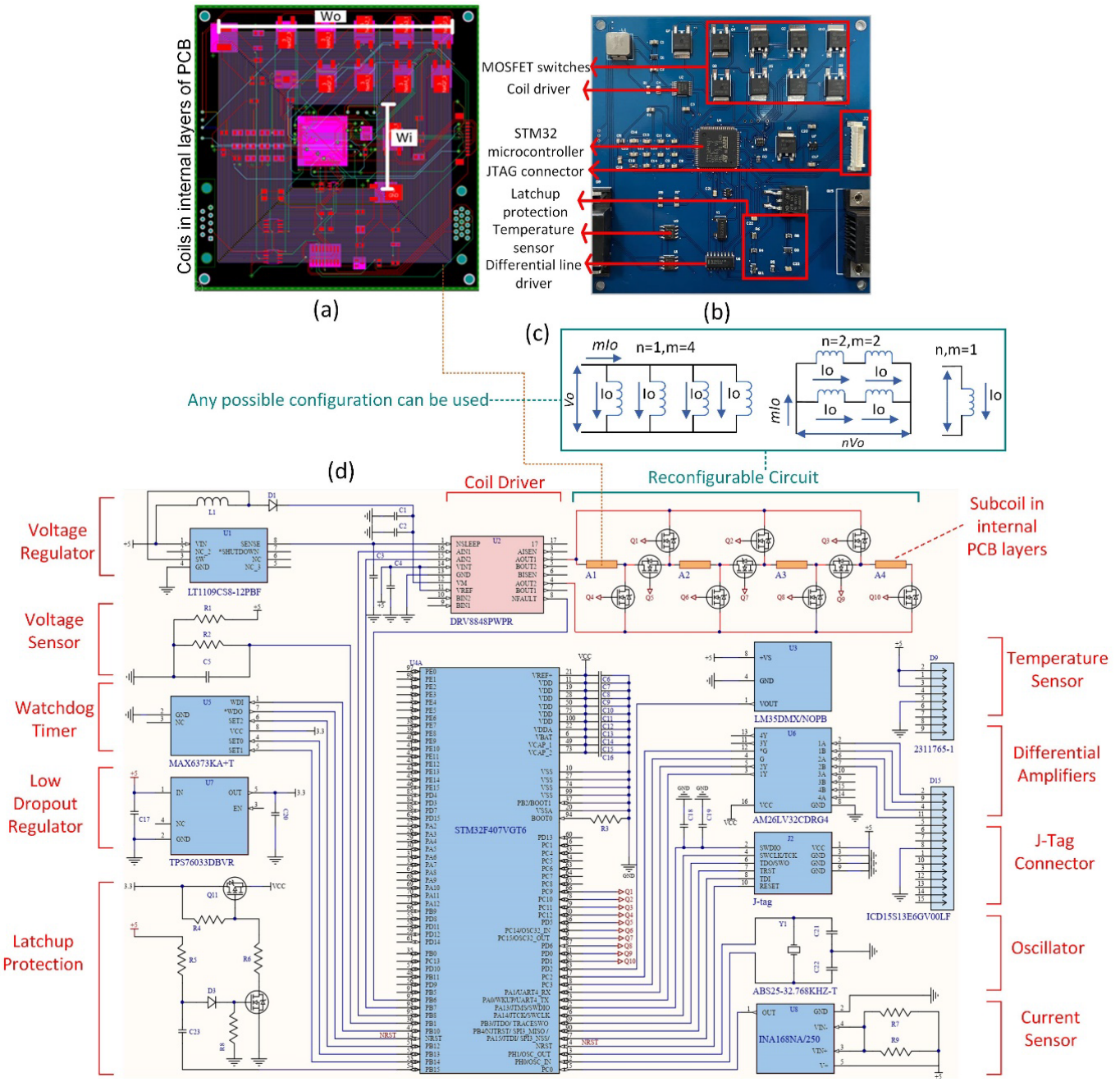

Fig. 2(a) Planar coils embedded inside the multilayer PCB. (b) Coil driver module mounted on the bottom side of PCB **(c)** Voltages required for various configurations of coils that offer constant current. (d) Coil driver schematic

The magnetorquer coil driver unit is primarily built using COTS microdevices which are inexpensive and easily accessible from the market. The simple design basically allows the academic and private institutions to improve the system's viability and raise the developmental practices bar which provides the experimental knowledge and testbed for further promotion of the findings and educational experience.

The PCB-integrated magnetorquer driver module consist of MOSFETS based reconfigurable circuit, differential line drivers, Joint Test Action Group (JTAG) connector, Latch-up protection system, voltage regulators, housekeeping sensors (current, voltage and temperature) and STM32 microprocessor. PCB-Integrated magnetorquer driver prototype is fabricated to experimentally verify the reconfigurability of the designed planar coils.

The planar magnetorquers are integrated in the eight-layered solar panel PCB embedded inside the four inner layers that do not take any extra space on the spacecraft as depicted in Figure 2(a). The coils integrated inside the PCB coil driver prototype shown in Figure 2(b) are actuated for a range of voltages (1-12V) such as the power distribution buses used on the CubeSats platform. The Dual H bridge motor IC (DRV8848) supervises the magnetic actuation of planar coils by monitoring the amount and direction of current flow as a function of voltage applied. The IC features undervoltage-lockout (UVLO), short circuit overcurrent protection (OCP) and over temperature. A circuit having reconfigurable topology is mounted to the 'DRV8848' IC as shown in the PCB schematic featuring the spacecraft with reconfigurable attitude control maneuvering and modular system. The planar

coils shown in Figure 2(a) embedded inside the PCB are reconfigured through the MOSFETS switches shown in PCB schematic design through the reconfigurable circuit. Figure 1(c) shows that the coil can be configured in any possible arrangement (series, parallel and hybrid) by controlling the switches through the STM32 microprocessor. The arrangement is changed through the onboard processor by utilizing the additional configurability features which provides more flexibility to the design aspects of the system. Telemetry processor unit (TPU) is utilized to transmit the telemetry data points for intercommunication with ground station controlled through the OBC monitoring the required generated torque, dipole moments produced or consumption of power by the planar coils. Figure 2(d) illustrates the coil driver schematic.

The coil driver module communicates with the spacecraft's OBC through the differential line drivers using redundant dual CAN system for all the telemetries and telecommands interconnected with DB9 connectors. They feature sufficient number of telemetries (using redundant can bus protocol) to manage and sustain the desired consumption of power of the overall coil driver unit. Noise immunity for precise and accurate control of bus communication at high switching frequencies featuring low power consumption without sacrificing the speed is achieved by these efficient differential line drivers developed for high input impedance and high hysteresis.

INA168 current sensor IC is used which is a high-side current measurement unipolar device that monitors the current as a function of differential voltage input and the data is sent through the telemetries managed by the STM32 microcontroller. Housekeeping (temperature and voltage) sensors are used to regulate the planar coils consumption of power and the rise of temperature gradients.

A watchdog timer is installed for robustness which externally controls the activity of the "STM32" microprocessor and a pulse is triggered in case of an anomaly to reset the tiles' onboard processor. JTAG (Picoblade) test access port is employed in the board design to allow the user for testing and debugging of the module. A Latch-up protection system is built and adopted based on the design in [26] for reducing the probability of a radiation-induced Latch-up. This is done because of the cosmic radiations in space which makes the complementary metal–oxide–semiconductor (CMOS) based COTS microdevices susceptible to latch-ups.

Montenbruck and Plfeger's (2000) method is used for modeling sun tracking. The torque commands are reiterated till the stability and orientation needed is sustained using a closed loop feedback. International geomagnetic reference field (IGRF) as is adopted to model the magnetic field.

3. Attitude equations of motion

A three coordinates or attitude parameters minimal set is needed for the representation of three-dimensional maneuvers of a rigid body. However, any minimal three-parameter set will experience singularities that must be taken into consideration, while more than three redundant parameters set could provide singularity free attitude representation at a cost of additional parameter constraints. The Euler angles as such represents a set of minimal three attitude parameters but the same orientations are given that lead to singularity in many ways. Therefore, the selection of the unit quaternion also known as the Euler Parameters (Eps) for redundant attitude coordinate set are motivated because of its singularity-free representation and rotational sequences which are computationally less expensive. Moreover, the direction cosine matrix requires more onboard processor power than the quaternions [27]. The orientation in space results from the kinematics based on the quaternion which is given by the numerical integration of angular velocity. Hence, the kinematics of quaternion are presented using the quaternions as shown in Eq. (1).

The transformation matrix is calculated as;

$$\begin{Bmatrix} \dot{q}_0 \\ \dot{q}_1 \\ \dot{q}_2 \\ \dot{q}_3 \end{Bmatrix} = \frac{1}{2} \begin{bmatrix} 0 & -p & -q & -r \\ p & 0- & r & -q \\ q & -r & 0 & p \\ r & q & -p & 0 \end{bmatrix} \begin{Bmatrix} q_0 \\ q_1 \\ q_2 \\ q_3 \end{Bmatrix} \tag{1}$$

Where four quaternions are represented by q_i and *p, q, r* denote the angular velocities in the body frame of the vehicle. The angular velocity's derivative is found by computing the angular momentum's derivative to the total moments subjected onto the vehicle.

$$\begin{Bmatrix} \dot{p} \\ \dot{q} \\ \dot{r} \end{Bmatrix} = [I]^{-1} \left(\begin{Bmatrix} L \\ M \\ N \end{Bmatrix} - \mathbf{S}(\vec{\omega}_{B/I})[I] \begin{Bmatrix} p \\ q \\ r \end{Bmatrix} \right) \tag{2}$$

Where **S**() stands for the skew symmetric operator and cross product is given by its multiplication with the vector.

$$S(\vec{\omega}_{B/I}) = \begin{bmatrix} 0 & -r & q \\ r & 0 & -p \\ -q & p & 0 \end{bmatrix} \tag{3}$$

The inertia tensor moment is denoted by *I* taken across the mass center in the body frame which is symmetric and positive. *L*, *M* and *N* are the magnetic moments which are control torques that provide rotation to the satellite as presented in Eq. (2). Torques that are parasitic in nature such as solar radiations, gravity, aerodynamic torques and residual magnetic dipoles are neglected for avoiding the computational complexity. Therefore, planar coils solely contribute to the total torques as given in Eq. (2).

3.1 Planar magnetorquer analytical model

The satellite is required to be controlled by a minimum of three set of planar coils (arranged in series, parallel or hybrid configuration) to actuate the satellite, mutually mounted perpendicular to each other in such a way, that every set of coils is lined up with *x*-, y and z-axis respectively. The magnetorquer coils are embedded in the innner layers of the multilayered PCB. When current passes through the planar coils in such a manner that $\vec{\imath}_B = \left[i_X, i_y, i_z\right]^T$, magnetic moment is subjected onto the spacecraft and each set of planar coils can be independently controlled. This generate a magnetic

dipole moment by the planar coils because the current passing through it couples with the Earth's magnetic field resulting in subjected torque. Equation (4) gives the magnetic dipole moment.

$$\overrightarrow{\mu_B} = nA\vec{\imath}_B \tag{4}$$

Where the number of turns of single planar coil is presented by n of each magnetorquer and A is area occupied by the planar coil in the PCB. The torque generated in the body reference frame by the planar coils is equated as the vector product of geomagnetic field with the magnetic moment.

$$\overrightarrow{\tau_B} = \mathbf{S}\,(\overrightarrow{\mu_B})\mathbf{T}(\overrightarrow{q})\,\vec{B}_I \tag{5}$$

The quaternion transformation matrix equates the vector of magnetic field in the body frame from the vehicle's inertial frame represented by $\mathbf{T}(\overrightarrow{q})$ which is depicted in the following equation.

$$\mathrm{T}(\overrightarrow{q}) = \begin{bmatrix} q_0^2+q_1^2-q_2^2-q_3^2 & 2(q_1q_2+q_0q_3) & 2(q_1q_3-q_0q_2) \\ 2(q_1q_2-q_0q_3) & q_0^2-q_1^2+q_2^2-q_3^2 & 2(q_1q_2+q_2q_3) \\ 2(q_0q_2+q_1q_3) & 2(q_2q_3-q_0q_1) & q_0^2-q_1^2-q_2^2+q_3^2 \end{bmatrix}$$

Equation (5) can be rewritten as Eq. (6) following the identity such that $\vec{a}\times\vec{b} = -\vec{b}\times\vec{a}$

$$\begin{Bmatrix} L \\ M \\ N \end{Bmatrix} = nA \begin{bmatrix} 0 & B_z & -B_y \\ -B_z & 0 & B_x \\ B_y & -B_x & 0 \end{bmatrix} \begin{Bmatrix} i_x \\ i_y \\ i_z \end{Bmatrix} \tag{6}$$

Where the components of magnetic field in the satellites' body frame are represented by B_X, B_y, B_z.

The generated magnetic dipole moments and the corresponding dissipated power for various arrangement of coils are revisited [22,23]. single coil's magnetic moment is given by $\overrightarrow{D_0}$. For any required configuration (m-parallel, n-series, n × m-hybrid), the magnetic dipole moment of M planar coils is denoted by $\vec{D}$ and equated as;

$$\vec{D} = M\overrightarrow{D_0} \tag{7}$$

Similarly, the Power consumed P_0 by single coil is represented as;

$$P_0 = I_0^2 R_0 \quad \because R_0 = \rho\frac{L_t}{A}$$

Power dissipation of M coils configured in any required configuration (n-series, m-parallel, n × m-hybrid) is;

$$P = MP_0 \tag{8}$$

a

$$\because I = mI_0\,,\, V = nV_0\,,\, M = n\times m$$

When the number of coils in a series, parallel, or hybrid configuration increases, so does the magnetic moment and power dissipation. The voltage is constant in case of the parallel-connected coils and the current flowing through the coils remains the same in case of single or series arrangement with similar generated torque.

3.2 B-dot controller

The projection based form of B-dot controller is utilized which follows a simple control law that compares the detumbling rates and behavior of the small satellites using the PCB-integrated reconfigurable coils as shown in Eq. (9). The B-dot controller basically uses the vicious friction of the satellites' rotational positions relevant to the Earth magnetic field vector B. Equation (9) represent the control law [28];

$$\overrightarrow{\mu_B} = K\mathbf{S}\,(\vec{\omega}_{B/I})\,\mathbf{T}(\overrightarrow{q})\,\vec{B}_I \tag{9}$$

Where the scalar control gain factor is denoted by K. The vehicles' kinetic energy is slowed or reduced when the controller effectively exerts torque in the direction perpendicular to both the angular velocity and magnetic field. The equation basically depicts that the angular velocities per orbit can be reduced by the control gain of the scalar product with time varying geomagnetic field. The currents are represented in the components form from Eq. (4) by using the identity that $\vec{a}\times\vec{b} = -\vec{b}\times\vec{a}$.

$$\begin{Bmatrix} i_x \\ i_y \\ i_y \end{Bmatrix} = \frac{K}{NA} \begin{bmatrix} 0 & B_z & -B_y \\ -B_z & 0 & B_x \\ B_y & -B_x & 0 \end{bmatrix} \begin{Bmatrix} p \\ q \\ r \end{Bmatrix} \tag{10}$$

$$\begin{Bmatrix} L \\ M \\ N \end{Bmatrix} = -K \begin{bmatrix} B_y^2 + B_z^2 & -B_xB_y & -B_xB_z \\ -B_xB_y & B_x^2 + B_z^2 & -B_YB_z \\ -B_xB_z & -B_yB_Z & B_x^2 + B_y^2 \end{bmatrix} \begin{Bmatrix} p \\ q \\ r \end{Bmatrix} \tag{11}$$

Spacecraft's total torque is computed by substituting Eq. (10) into Eq. (6) under the assumption that the planar coils could generate the required current.

The objective is to detumble the small satellite, damp the body rates and make the angular rates to almost null. The reaction wheels are usually used to offer three-axis attitude control autonomously (deploying three wheels) without relying on external applicators of torque, generating the torque in the local Earth's magnetic field vector as the PCB integrated planar coils cannot produce this torque component. However, during the detumbling phase, the rotations of the satellite are around all the axes subjected to the varying Earth's magnetic field influence. Hence, whenever the velocity $\vec{\omega}_B$ is not parallel to $\vec{B}_I$, the B-dot controller can effectively keep decreasing the vehicle's angular momentum. Moreover, as mentioned before, the planar coils are embedded

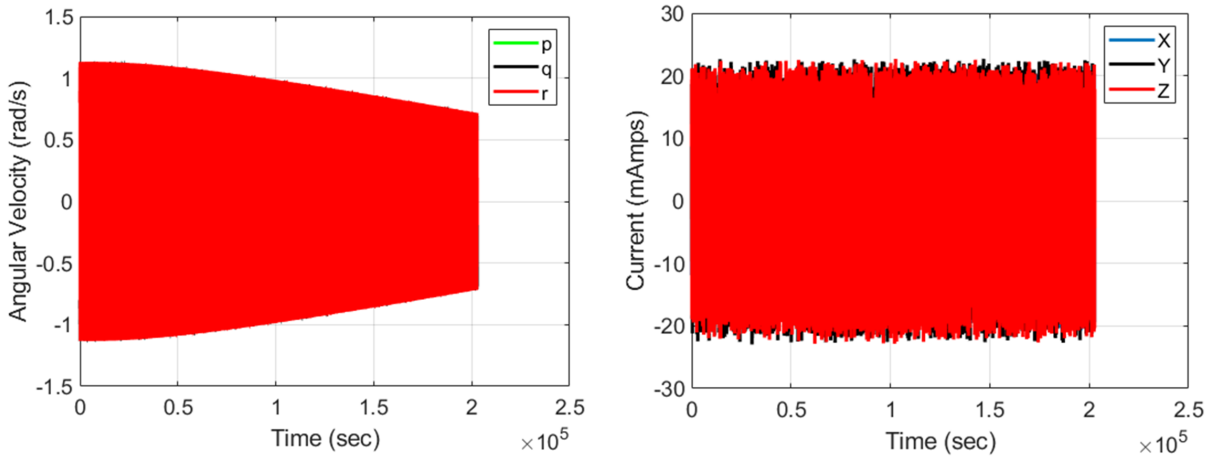

(a) (b)

Fig. 6 (a) 4U spacecraft's pitch, yaw and roll rate (rad/s) vs. time (s) for single coil (1x1). Fig. 6 (b) 4U spacecraft's current drawn in pitch, yaw and roll axes for single coil (1x1)

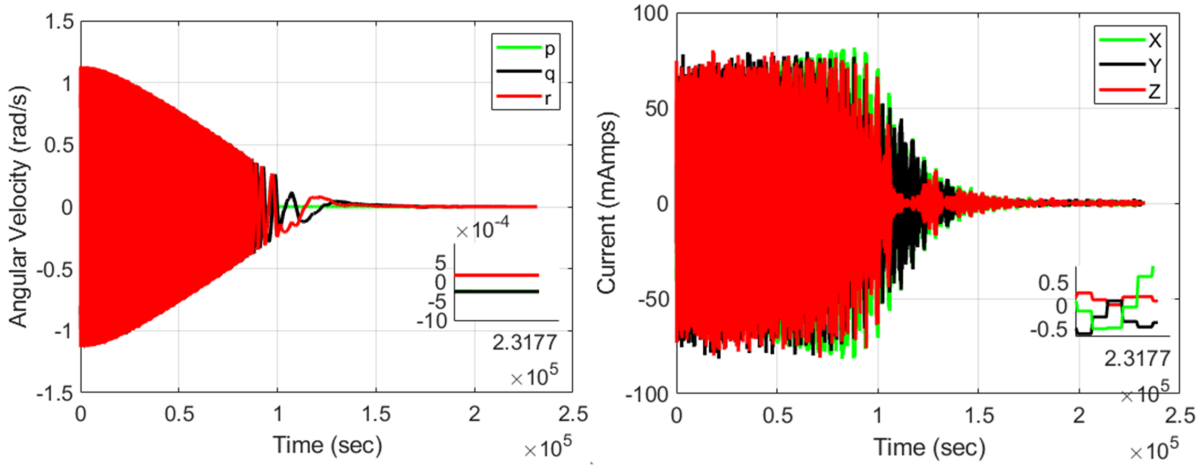

(a) (b)

Fig. 7 (a) 4U spacecraft's pitch, yaw and roll rate (rad/s) vs. time (s) for parallel configuration (1x4). Fig. 7 (b) 4U spacecraft's current drawn in pitch, yaw and roll axes for hybrid configuration (1x4)

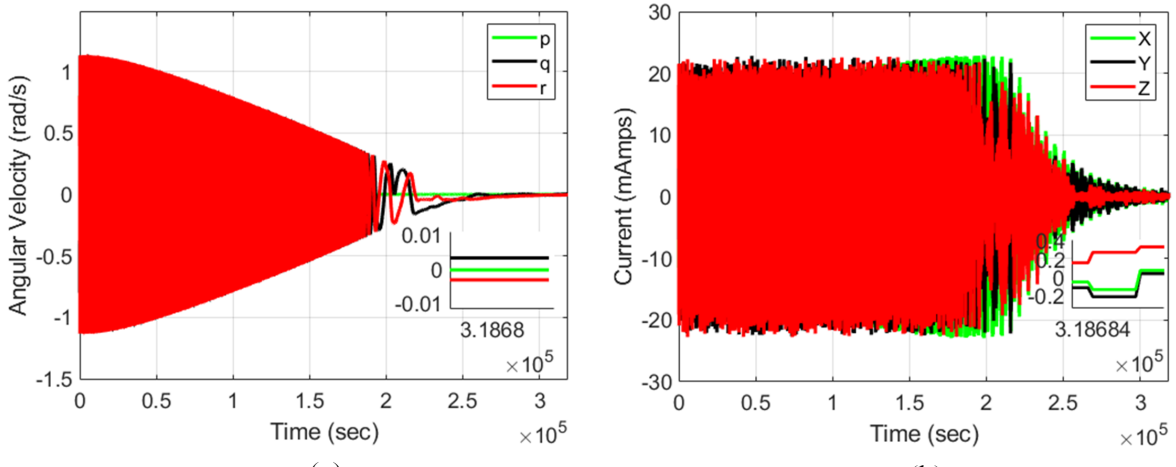

(a) (b)

Fig. 8 (a) 4U spacecraft's pitch, yaw and roll rate (rad/s) vs. time (s) for hybrid configuration (2x2). Fig. 8 (b) 4U spacecraft's current drawn in pitch, yaw and roll axes for hybrid configuration (2x2)

spacecraft's current drawn in pitch, yaw and roll axes for hybrid configuration (2x2)

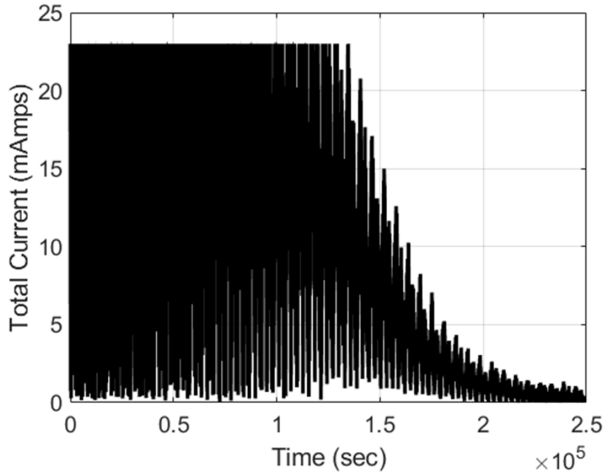

Fig. 9 Total current drawn by magnetorquers through single coil (1x1) for 2U vehicle

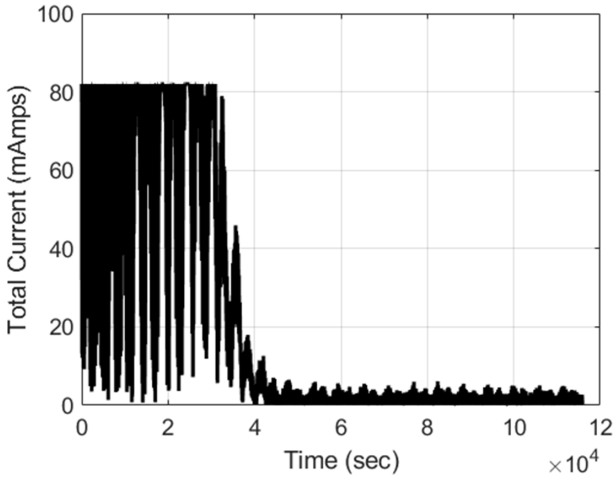

Fig. 10 Total current drawn by magnetorquers in parallel arrangement (1x4) for 2U vehicle

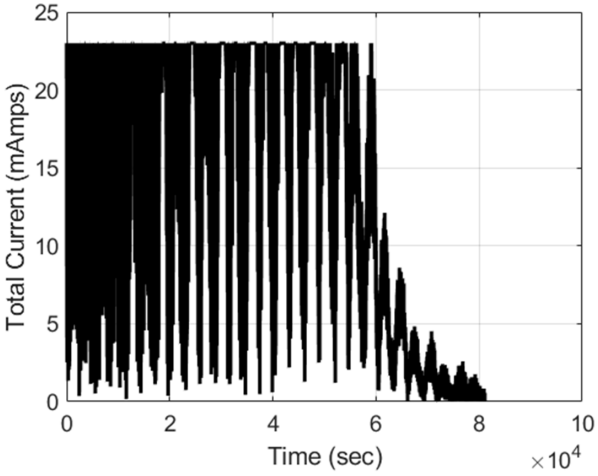

Fig. 11 Total current drawn by magnetorquers in hybrid configuration (2x2) for 2U vehicle

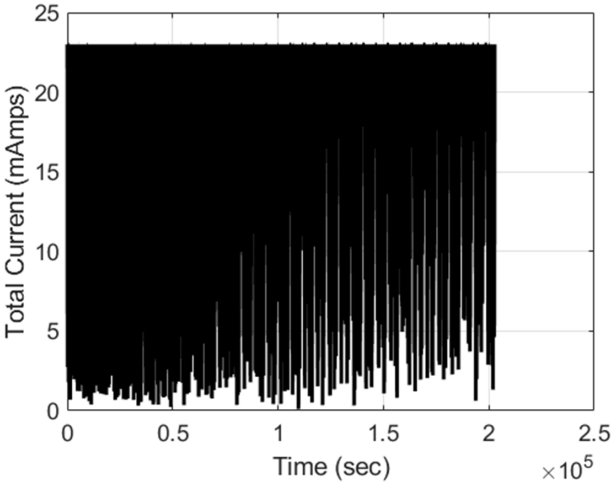

Fig. 12 Total current drawn by magnetorquers through single coil (1x1) for 4U vehicle

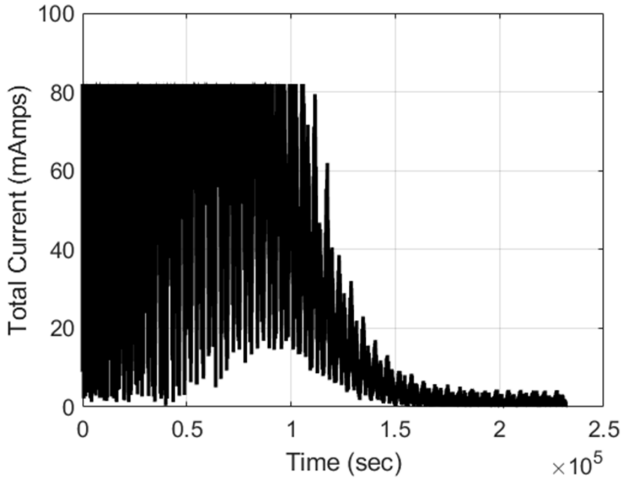

Fig. 13 Total current drawn by magnetorquers in parallel configuration (1x4) for 4U vehicle

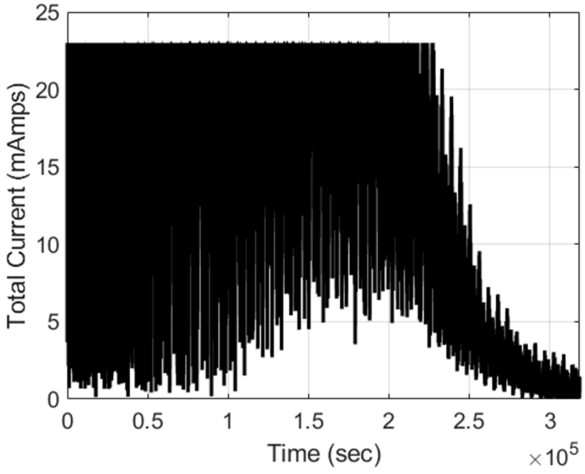

Fig. 14 Total current drawn by magnetorquers in hybrid arrangement (2x2) for 4U vehicle

inside the PCB which act as magnetorquers and the coil driver is mounted at the bottom side of the solar panel PCB that will

not take any additional space. Therefore, only three solar panel PCBs placed on the output periphery of the satellite orthogonally along the x, y and z axes shall offer the three-dimensional maneuverability without the need of costly and bulky reaction wheels.

4. Small satellites detumbling analysis

The satellites are modeled after 2U and 4U dimensions of $10\times 10\times 20\ \text{cm}^3$ and $10\times 10\times 40\ \text{cm}^3$ carrying a mass of 5kg and 7kg respectively. For 2U and 4U spacecraft, the inertia is set to $I_X = 0.0083$ and $I_Y = I_z = 0.0208\ \text{kgm}^2$ and $I_X = 0.0117$ & $I_Y = I_z = 0.0992\text{kgm}^2$ respectively. We perform the orbital simulations for placing the vehicle in an orbit at 600km above the earth surface with an inclination angle of 56°

The satellite's initial angular rate of velocity is set to [0.8, -0.8, 08] (rad/s). Fixed step fourth-order Runge-Kutta (RK4) integration routine is followed for carrying out the orbital simulations having a timestep of 0.1. For achieving the three-dimensional maneuverability, it is assumed that the current can be passed in both the directions of the planar coils utilizing the dual H-bridge motor driver IC as discussed in the coil driver section. Equation (12) is used to compute the controller gain *K* based on the design parameters of different possible coil arrangements (n×m). Number of turns in single layer are 55. The current drawn of single coil is 0.023A, parallel arrangement (1×4) is 0.082A and the hybrid arrangement (2×2) is 0.023A. The total current of planar magnetorquers cannot exceed these ratings. Authors recommend to revisit ref [22] for more details about the performance parameters of the coils. It is important to note that the resulting current generated by the planar coils will be zero according to Eq. (9) if the magnetic moment vector or angular velocity vector are collinear. Therefore, the torque applied to the spacecraft will consequently be zero according to (12). However, pragmatically this usually does not happen since the Earth's magnetic field is time and spatially varying that is changing over the duration of time due to satellite's tumbling over all axes or the orbital changes experienced by the vehicle. The embedded coils inside the PCB have current ratings depending upon the type of coil arrangements (n×m) used.

In the case of 2U spacecraft, all the possible circuit topologies detumble the spacecraft without the significant computational burden as depicted in Figures 3-5. Series configuration (4×1) needs more time for detumbling the spacecraft because of the reduced current drawn and low power consumption characterized by its circuit topology whereas the hybrid (2×2) configuration detumble the satellite significantly faster because of the higher current drawn comparatively. The least amount of time required for detumbling the vehicle is taken by the parallel configuration (1×4) but at the expense of higher power consumption for all the satellites due to the highest current drawn by its circuit topology. In the case of 4U spacecraft, the series configuration (4×1) cannot remove the body rates from the satellite while the hybrid configuration (2×2) struggles in removing the body rates effectively in comparison with the parallel configuration (1×4) as shown in Figures 6-8. The parallel configuration (1×4) removes the angular velocities from the spacecraft proficiently in lesser time. It is evident that the torque applied to detumble the spacecraft is inversely proportional to the time taken. Therefore, parallel arrangement (1×4) offers rotation to the satellite in the least amount of time with the highest generated torque. Furthermore, it is also clear that by increasing the dimensions of satellites to larger cube units, higher torque is required by the vehicle for removing the tumbling rates effectively. Therefore, higher number of copper layers could be integrated internal to the PCB for improving the generated torque and subsequently attaining the steady state angular rates if efficient detumbling capabilities are demanded. Figures 9-14 shows the total current of magnetorquers drawn over the course of detumbling timespan.

The selection of coil configuration basically is dependent upon the required power consumption of the mission objectives. Small satellites having higher inertia when subjected to prolonged detumbling can significantly affect the structural integrity and performance of the sensitive payloads they carry. Therefore, the vehicle should be detumbled in least amount of time. In both the cases (2U and 4U) under study, the authors recommend to use the parallel arrangement (1×4) as they offer optimal detumbling capabilities with reasonable power consumption and the temperature rise of the planar coils is within the thermal equilibrium as shall be discussed in the thermal analysis section.

5. Thermal analysis

The dissipated power and the resulting temperature rise of the PCB-Integrated reconfigurable embedded planar coils are calculated from the mathematical framework derived in [22] represented as following;

$$T_o = \sqrt[4]{\frac{P_d + \alpha\sigma {T_I}^4 S}{\alpha\sigma S}}\ , P_d = I^2R \qquad (12)$$

Whereas the surrounding temperature is represented by T_I, Stefan-Boltzmann constant is denoted by σ, the power dissipated inside the PCB by the planar coils is depicted by P_d, and solar panel module emissivity is presented by α which is given by Eq. (13).

$$\alpha = \frac{P_d}{\sigma S\left({T_o}^4 - {T_I}^4\right)} \qquad (13)$$

The solar panel module's surface emissivity value is measured experimentally in [22] using a measurement setup that is used for the comparison of T_o for different possible configuration of planar coils. The trace thickness & width

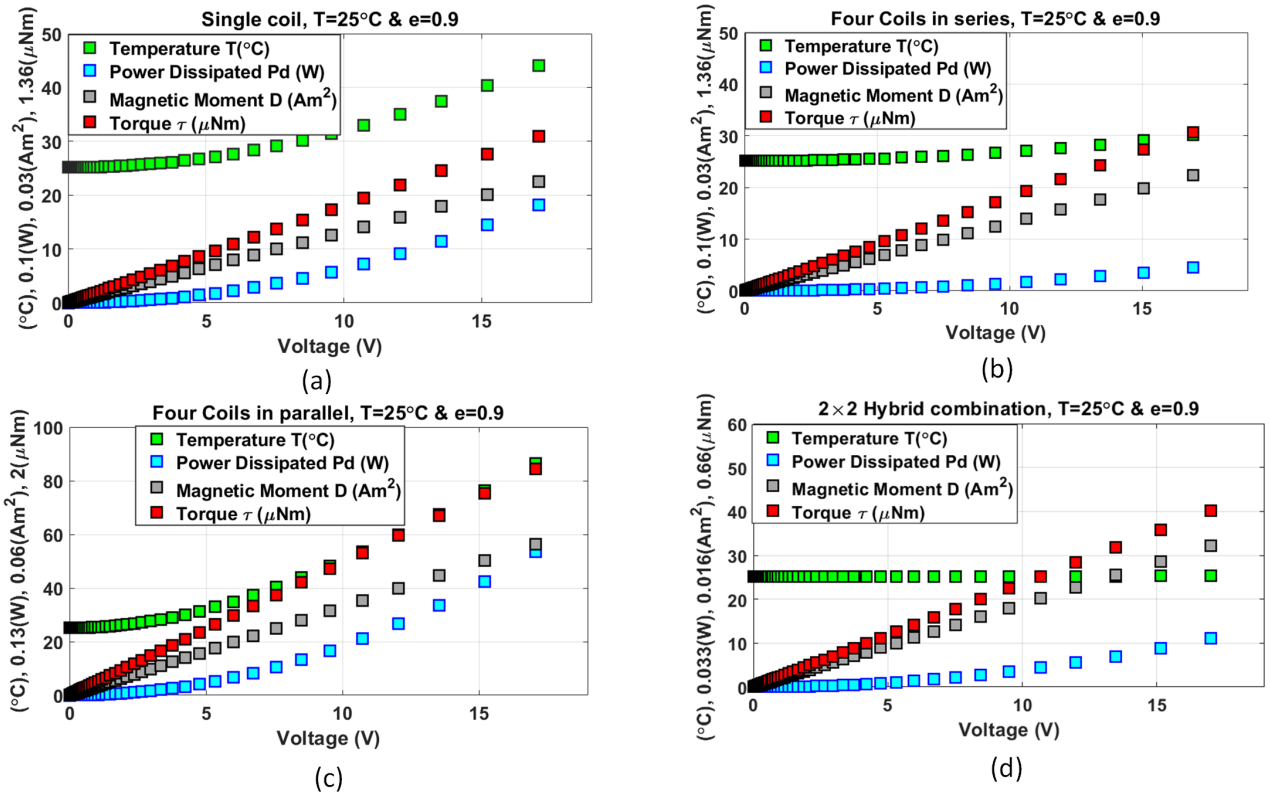

Fig. 15 Planar magnetorquers' performance parameters of 2U spacecraft for various configurations against applied voltage

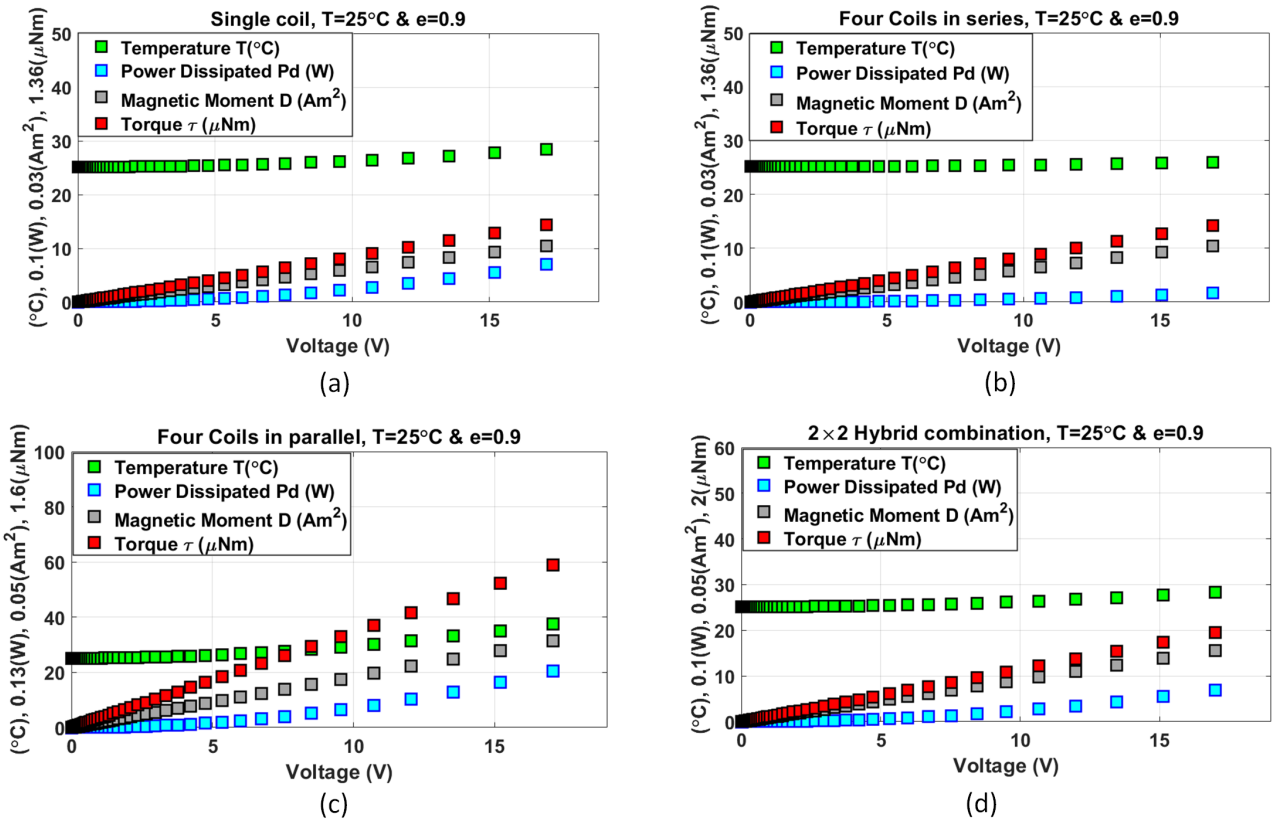

Fig. 16 Planar magnetorquers' performance parameters of 4U spacecraft for various configurations against applied voltage

Table 1. Planar magnetorquers' performance parameters for different possible arrangements compared with the commercial state-of-the art

Attitude control system		Price	Mass (g)	Dimension (mm)	P (W)	τ (μNm)	$\frac{\tau}{P}$
Commercial designs	Gomspace Nanopower (P110) [29]	PCB inner layers	57 g	No space occupation	2.3	0.82	0.35
	Magnetorquer rod (NCTR-M012) [30]	$2000	50 g	94×15×13	0.9	60	66
Embedded planar magnetorquer	(1×4) Coils in parallel	PCB inner layers	81.2g	No space occupation	0.32	18.64	58.25
	(2×2) Coils in hybrid	PCB inner layers	81.2g	No space occupation	0.08	9.2	115
	(4×1) Coils in Series	PCB inner layers	81.2g	No space occupation	0.02	4.3	215

material used and the number of turns significantly affect the temperature rise of the coils inside the PCB. The torque generation and the respective magnetic dipole moment imparted to the spacecraft can be increased with the increase in the number of turns, trace width & thickness and the decrease in resistance with the subsequent increase in rise of temperature and power dissipation of the overall module. Series arrangement gives the optimal torque versus power dissipation ratio as it draw very low current and thus dissipates less power. The analysis shows that when the dimensions of the vehicle are increased, the torque and magnetic dipole moment increases as well and the power dissipation and its corresponding temperature gradients decrease. The thermal analysis results show that all the configurations of the planar magnetorquers can generate reasonable torque for the detumbling maneuvers of small satellites except for the series configuration in the case of a 4U vehicle.

The analyses are done for the range of 18V inputs applied to spacecraft with dimensions of 2U and 4U respectively such as those used on CubeSats power distribution buses as shown in Figures 5 and 6. The values derived in this section are for 3.5V inputs. In case of single coil (1×1), magnetic moment generated is 0.09 Am^2 & 0.18 Am^2, the power dissipated is 0.08 W & 0.05 W, generated torque is 4.6 μNm & 9.31 μNm, PCB temperature rise is 26.5 ˚C & 26.1 ˚C for 2U and 4U small satellites respectively. In case of series configuration (4×1), magnetic moment generated is 0.09 Am^2 & 0.18 Am^2, power dissipated is 0.02 W & 0.9 W, generated torque is 4.6 μNm & 9.31 μNm, PCB temperature rise is 25.8 ˚C & 25.2 ˚C for 2U and 4U small satellites respectively. In case of parallel configuration (1×4), magnetic moment generated is 0.38 Am^2 & 0.74 Am^2, power dissipated is 0.32 W & 0.27 W, generated torque is 18.64 μNm & 37.27μNm, PCB temperature rise is 30.2 ˚C & 29.1 ˚C for 2U and 4U small satellites respectively. For hybrid configuration (2×2), magnetic moment generated is 0.18 Am^2 & 0.37 Am^2, power dissipated is 0.08 W & 0.05 W, generated torque is 9.2 μNm & 18.5μNm, PCB temperature rise is 26.7 ˚C & 26.1 ˚C for 2U and 4U small satellites respectively.

Single coil (1×1) and series configuration (4×1) generate the same magnetic dipole moment & torque but the series arrangement consumes significantly less power that corresponds to its lower thermal envelope as well. In light of this, any number of the planar coils can be embedded inside the PCB for minimizing the power consumption of the magnetorquer module depending upon the requirements of the mission. The single (1×1) and hybrid (2×2) configuration dissipates the same power but the hybrid arrangement generates more torque and dipole moment. The maximum torque and dipole moment is given by the parallel arrangement (1×4) but at the expense of higher power consumption and temperature rise of the module. The temperature rise of parallel configuration (1×4) in case of a 2U and 4U spacecraft is 30.2 ˚C and 29.1˚C that are the steady state temperatures when the planar coils are energized for a longer span of time. Furthermore, the switching configuration controlled through the onboard processor allows the consumer to efficiently use the different arrangement topologies during detumbling phase to sustain the temperatures in real time. The temperature rise of coil configurations in case of 4U spacecraft is slightly less than the 2U spacecraft because of the larger surface area, thus, entrapping less heat than the 2U vehicle. It is clear from the plots of Figures 15 and 16 that overall temperatures of the coils increase at higher operating voltages but remains within the thermal equilibrium at lower operating voltages even for the poor case of parallel arrangement (1×4). Therefore, lower operating voltages as a design selection should be chosen for designing the coils. It can thus be concluded that these PCB integrated magnetorquers based on planar coils can effectively remove the body rates of higher form factor small satellites. Table 1 tabulates the key performance parameters of planar

magnetorquer coils for different possible arrangements in comparison with the commercial state-of-the-art.

6. Conclusion

The embedded magnetorquers are gaining popularity in the area of ultraminiaturized satellites when it comes to layout area, lower power consumption, modularity, reasonable attitude maneuvering capabilities and the ease of integration with standard circuit design. Significant research is being carried out in terms of their optimizations to make them cheaper, smarter, smaller and faster. However, no efforts have focused on representing the embedded planar coils for their detumbling capabilities. The prototype built by Surrey Space Centre involved a PCB-Sat; where the spacecraft is designed on a single PCB and Chip-Sat; where the spacecraft is designed in a single chip. Currently they are being built at Surrey Space Centre where these ultraminiaturized complete vehicles will be beneficial for the distributed spacecraft space missions in the future. Similarly, the PCB-Integrated reconfigurable embedded planar coils which are almost massless could play a crucial role in proving to be a reliable attitude control system. These planar coils can damp out the high angular rates of tumbling small satellites in LEO. The detumbling results guaranteed the three-axis stability utilizing the three sets of embedded planar coils for purely magnetic fast detumbling CubeSats when application specific coil configurations were used. The dipole moment to power dissipation ratio demonstrated by the embedded planar coils outperforms the commercial state of the art.

Conflict of interest

The authors declare that they have no conflict of interest.

References

[1] A. Poghosyan, A. Golkar, CubeSat evolution: Analyzing CubeSat capabilities for conducting science missions, Prog. Aerosp. Sci. (2017). https://doi.org/10.1016/j.paerosci.2016.11.002.

[2] S. Chen, H. Lin, G. Yang, Efficient agricultural disaster financing using satellite data and artificial intelligence, Comput. Electr. Eng. 103 (2022) 108394. https://doi.org/https://doi.org/10.1016/j.compeleceng.2022.108394.

[3] J.R. Kopacz, R. Herschitz, J. Roney, Small satellites an overview and assessment, Acta Astronaut. (2020). https://doi.org/10.1016/j.actaastro.2020.01.034.

[4] H.J. Kramer, A.P. Cracknell, An overview of small satellites in remote sensing, Int. J. Remote Sens. (2008). https://doi.org/10.1080/01431160801914952.

[5] M. O'Halloran, J.G. Hall, L. Rapanotti, Safety engineering with COTS components, Reliab. Eng. Syst. Saf. 160 (2017) 54–66. https://doi.org/https://doi.org/10.1016/j.ress.2016.11.016.

[6] A. Ali, S.A. Khan, M.A. Dildar, H. Ali, N. Ullah, Design & thermal modeling of solar panel module with embedded reconfigurable Air-Coil for micro-satellites, PLoS One. (2018). https://doi.org/10.1371/journal.pone.0199145.

[7] S. Ahmed Khan, A. Ali, Y. Shiyou, J. Tong, J.M. Guerrero, Optimized Design of Embedded Air Coil for Small Satellites with Various Dimensions, J. Aerosp. Inf. Syst. (2021). https://doi.org/10.2514/1.i010882.

[8] A. Golkar, A. Salado, Definition of New Space—Expert Survey Results and Key Technology Trends, IEEE J. Miniaturization Air Sp. Syst. (2020). https://doi.org/10.1109/jmass.2020.3045851.

[9] K. Gaber, M.B. El_Mashade, G.A.A. Aziz, Hardware-in-the-loop real-time validation of micro-satellite attitude control, Comput. Electr. Eng. (2020). https://doi.org/10.1016/j.compeleceng.2020.106679.

[10] A.K. Shoaib, A. Anwar, S. Yang, F. Shah, T. Jijun, Optimized Design and Analysis of Printed Magnetorquer for a 3-U Nano-Satellite, J. Aerosp. Eng. 35 (2022) 4021103. https://doi.org/10.1061/(ASCE)AS.1943-5525.0001343.

[11] H.S. Ousaloo, Magnetic attitude control of dynamically unbalanced spinning spacecraft during orbit raising, J. Aerosp. Eng. (2014). https://doi.org/10.1061/(ASCE)AS.1943-5525.0000252.

[12] M. Zhu, X. Chen, Z. Li, Attitude and momentum management of inertial oriented spacecraft, J. Aerosp. Eng. (2015). https://doi.org/10.1061/(ASCE)AS.1943-5525.0000471.

[13] S. Ahmed Khan, A. Ali, Y. Shiyou, J. Tong, Reconfigurable Asymmetric Embedded Magnetorquers for Attitude Control of Nanosatellites, IEEE J. Miniaturization Air Sp. Syst. (2021). https://doi.org/10.1109/JMASS.2021.3094232.

[14] M. Lovera, A. Astolfi, Global magnetic attitude control of spacecraft in the presence of gravity gradient, IEEE Trans. Aerosp. Electron. Syst. (2006). https://doi.org/10.1109/TAES.2006.248214.

[15] L. Sun, Z. Wang, G. Zhao, H. Huang, Magnetic attitude tracking control of gravity gradient microsatellite in orbital transfer, Aeronaut. J. (2019). https://doi.org/10.1017/aer.2019.112.

[16] E. Gill, P. Sundaramoorthy, J. Bouwmeester, B. Zandbergen, R. Reinhard, Formation flying within a constellation of nano-satellites: The QB50 mission, Acta Astronaut. (2013). https://doi.org/10.1016/j.actaastro.2012.04.029.

[17] S. Ahmed khan, Y. Shiyou, A. Ali, S. Rao, W. Jing, S. Fahad, J. Tong, Active Attitude Control for Microspacecraft; A Survey and New Embedded Designs, Adv. Sp. Res. (2022). https://doi.org/https://doi.org/10.1016/j.asr.2022.02.020.

[18] A. Sengupta, Magnetic confinement in a ring-cusp ion thruster discharge plasma, J. Appl. Phys. (2009). https://doi.org/10.1063/1.3106087.

[19] T. Morris, M. Jugroot, Study of an electrostatic micropropulsion system for nanosatellites, Can. Aeronaut. Sp. J. (2011). https://doi.org/10.5589/q11-017.

[20] N. Yamamoto, H. Masui, H. Kataharada, H. Nakashima, Y. Takao, Antenna configuration effects on thrust performance of miniature microwave discharge ion engine, J. Propuls. Power. (2006). https://doi.org/10.2514/1.18833.

[21] M. Tafazoli, A study of on-orbit spacecraft failures, Acta Astronaut. (2009). https://doi.org/10.1016/j.actaastro.2008.07.019.

[22] A. Ali, M.R. Mughal, H. Ali, L.M. Reyneri, M.N. Aman, Design, implementation, and thermal modeling of embedded reconfigurable magnetorquer system for nanosatellites, IEEE Trans. Aerosp. Electron. Syst. (2015). https://doi.org/10.1109/TAES.2015.130621.

[23] M.R. Mughal, H. Ali, A. Ali, J. Praks, L.M. Reyneri, Optimized Design and Thermal Analysis of Printed Magnetorquer for Attitude Control of Reconfigurable Nanosatellites, IEEE Trans. Aerosp. Electron. Syst. (2020). https://doi.org/10.1109/TAES.2019.2933959.

[24] M. Lovera, Magnetic satellite detumbling: The b-dot algorithm revisited, in: Proc. Am. Control Conf., 2015. https://doi.org/10.1109/ACC.2015.7171005.

[25] A.K. Sanyal, Z. Lee-Ho, Attitude tracking control of a small satellite in low earth orbit, in: AIAA Guid. Navig. Control Conf. Exhib., 2009. https://doi.org/10.2514/6.2009-5902.

[26] A. Ali, S.A. Khan, M. Usman Khan, H. Ali, M. Rizwan Mughal, J. Praks, Design of modular power management and attitude control subsystems for a microsatellite, Int. J. Aerosp. Eng. (2018). https://doi.org/10.1155/2018/2515036.

[27] J.L. Junkins, H. Schaub, Analytical Mechanics of Space Systems, Second Edition, New York, 2009. https://doi.org/10.2514/4.867231.

[28] M. Monkell, C. Montalvo, E. Spencer, Using only two magnetorquers to de-tumble a 2U CubeSAT, Adv. Sp. Res. (2018). https://doi.org/10.1016/j.asr.2018.08.041.

[29] GomSpace, p110 High effeciency solar panels, CubeSatShop. (n.d.). https://gomspace.com/UserFiles/Subsystems/datasheet/gs-ds-nanopower-p110-210.pdf (accessed February 9, 2023).

[30] NCTR-M012, NCTR-M012 Magnetorquer Rod, CubeSatShop. (n.d.). https://www.cubesatshop.com/product/nctr-m012-magnetorquer-rod/ (accessed June 4, 2020).

Shoaib Ahmed Khan received his B.S and M.S degree in Electrical Engineering from NUCES FAST, Pakistan, in 2014 and 2017 respectively. Since September, 2019, he is working as a PhD scholar at the Department of Electrical Engineering, Zhejiang University, Hangzhou, China. He has published many papers in renowned journals. His research interests include Design and Development of Aerospace Systems & Power Electronics.

SHIYOU YANG is a full Professor at the College of Electrical Engineering, Zhejiang University since 2001. Currently, his research interests include computational Electromagnetics in both high and low frequency domains, the application of numerical techniques in electronic and electromagnetic devices. So far, he has published more than 200 papers in referred international conference and journals, and more than 100 in high rank international journals.

Anwar Ali received his M.S. and Ph.D. degree in Electronic and Communication Engineering from Politecnico di Torino, Italy in 2010 and 2014, respectively. He is working as lecturer in Electronic Engineering Department, Swansea University, UK. His research interest is power electronics, embedded systems and spacecraft engineering. Dr. Anwar has published 44 research papers in leading international journals and conference proceedings.

Mustafa Tahir received the M.S. degree in electrical engineering from Nanjing University of Aeronautics and Astronautics, Nanjing, China, in 2020. He is currently pursuing the Ph.D. degree in electrical engineering at Zhejiang University, Hangzhou, China. He was a awarded of the excellent paper award by the IACGN in 2019 and the university scientist award by PCIM in 2022.

Shah Fahad received the B.S. and M. S. degrees from University of Peshawar, Peshawar, KPK, Pakistan, in 2014 and 2018 respectively. He is currently pursuing the Ph.D. degree in College of Electrical Engineering, Zhejiang University, Hangzhou, China. His research interests include Power Electronics, IoT smart transportation, QPSO and PSO.

Shaowei Rao was born in Ganzhou, China, in 1995. He received the B.Eng. degree in electrical engineering from Qingdao University in 2016, and M.Eng. degree in electrical engineering from China Electric Power Research Institute in 2019, respectively. He is currently pursuing his Ph. D. degree in electrical engineering at Zhejiang university. His major interests are in optimization and machine learning.

Muhammad Waseem received the M.Sc. and Ph.D degrees in electrical engineering from the University of Engineering and Technology Taxila, Pakistan and Zhejiang University, China in 2017 and 2022, respectively. His research interests include Optimizations, power system analysis, demand side management, distributed generation resources, and smart grids.